Journal of Catalysis **203,** 307–321 (2001)
doi:10.1006/jcat.2001.3337, available online at http://www.idealibrary.com on IDEAL®

Preparation of Highly Dispersed Pt Particles in Zeolite Y with a Narrow Particle Size Distribution: Characterization by Hydrogen Chemisorption, TEM, EXAFS Spectroscopy, and Particle Modeling

J. de Graaf, A. J. van Dillen, K. P. de Jong, and D. C. Koningsberger[1]

Department of Inorganic Chemistry and Catalysis, Debye Institute, Utrecht University, P.O. Box 80083, 3508 TB Utrecht, The Netherlands

Received January 30, 2001; revised May 22, 2001; accepted July 7, 2001

Research on metal–support interaction calls for highly dispersed metal particles inside the zeolite with a narrow particle size distribution. Pt particles thus dispersed in zeolite Y are obtained in this work using both ion exchange and dry impregnation techniques. For both preparation techniques a very low heating rate during calcination turns out to be essential. This low heating rate of 0.2°C/min leads to particles with an EXAFS Pt–Pt coordination number of 5–6, i.e., particles of 13–20 atoms, i.e., smaller than 1.1 nm. A rate of 1°C/min as used in the literature already leads to a bimodal particle size distribution. About 5 wt% large particles of 4–9 nm is (partially) occluded in the zeolite. Ninety-five weight percent of the Pt particles have an average size of 1–1.2 nm. The necessity to use a very low heating rate is explained by the slow desorption of water and ammonia from the microporous zeolite in combination with the stabilization of mobile Pt species by the cavity walls of the zeolite. The particle size distribution reported could be obtained only by combining the results of hydrogen chemisorption, TEM, EXAFS, and modeling of Pt particles.

Key Words: **Pt in Y; particle size distribution; rate of calcination; impregnation; ion exchange; TEM, H/Pt, EXAFS.**

INTRODUCTION

Supported noble metal catalysts are used in a large number of commercially important applications, including hydrogenation, dehydrogenation, naphtha reforming, isomerization, hydrocracking, oxidation, automotive exhaust catalysts, and fuel cells (1). Pt/Pd on zeolite Y catalysts are applied for such processes as deep hydrodesulfurization (HDS) and hydrodearomatization (HDA). The catalytic activity of supported metal catalysts for hydrogenation and hydrogenolysis is known to depend strongly on support properties such as (i) acidity/alkalinity, (ii) number and type of cations (iii) Si/Al ratio, and (iv) presence of extraframework Al (Al_{EF}).

To study the metal–support interaction in Pt/Y catalysts and to be able to discriminate between metal–support and particle size effects, a narrow particle size distribution of small platinum particles fitting the micropores of the zeolite is needed (2). Furthermore to study the metal–support interaction as a function of the different support compositions (Si/Al ratio, Na^+, H^+, Al_{EF}), the same narrow particle size distribution has to be present independent of the different support compositions.

Several procedures for the preparation of small metal platinum clusters from ion-exchanged zeolite Y are reported in the literature and the processes occurring during oxidation, decomposition, and reduction of the $Pt(NH_3)_4^{2+}$ complex have been investigated (8). To prepare well-dispersed platinum particles in zeolite Y, application of the $Pt(NH_3)_4^{2+}$ precursor ion via ion exchange of the zeolite is recommended (3–6). However, the effect of the method of application (ion exchange or impregnation) on the preparation result has not been extensively investigated.

To obtain metallic platinum particles, ultimately the precursor needs to be reduced. It is well known that treatment of the $Pt(NH_3)_4^{2+}$ ion-exchanged zeolite with hydrogen results in a very low platinum dispersion (3). The metal dispersion is markedly improved when the applied Pt complex is decomposed (7) or calcined prior to reduction (3). The resulting metal dispersion is reported to depend strongly on the calcination conditions. The best results are obtained when small amounts of ion-exchanged zeolite are calcined in a fixed bed reactor using a high oxygen-containing flow and a low heating rate. This was found both with zeolite Y and with ZSM 5 (3, 8, 9).

For characterization of the local structure, size, and location of platinum in zeolite NaY a number of techniques have been used: EXAFS, hydrogen chemisorption, HRTEM, and ^{129}Xe NMR (10). With EXAFS analysis particle size determination is accurate only if the metal particles are small and the particle size distribution is narrow. When the particle size distribution is broad or bimodal the larger particles dominate the average coordination number of the first Pt–Pt coordination shell. This means that the results obtained with EXAFS alone are not reliable. Analysis of (high-resolution) transmission electron micrographs is unique in

[1] To whom correspondence should be addressed. E-mail: d.c.koningsberger@chem.uu.nl. Fax: +31-302511027.

0021-9517/01 $35.00

providing directly the platinum particle size distribution. However, with TEM a lower limit of 1- to 2-nm platinum particles in zeolite Y is met because of the thickness of the Y crystals which leads to a considerable scattering contrast (11–14). Although HRTEM can be used on zeolite samples that are sliced by microtomy (11–14), a major problem is the amorphization of the zeolite and sintering of the metal particles under influence of the electron beam (14, 15).

In this article, the preparation of small platinum particles in zeolite (Y) is studied. Pt/NaY and Pt/H-USY are prepared by ion exchange or by impregnation of the zeolites with aqueous solutions of $Pt(NH_3)_4(NO_3)_2$. Special emphasis is attributed to the influence of the heating rate to reach the calcination temperature. To gain more insight into the influence of the microporosity of the zeolite on the finally obtained metal dispersions, a comparison is made with a mesoporous amorphous silica–alumina as the support. The platinum particle size distribution was determined by combining the results obtained with hydrogen chemisorption, TEM, and EXAFS.

Very small Pt particles having 13–20 atoms per particle and of an average size smaller than 1.1 nm are prepared in NaY and H-USY from ion-exchanged and impregnated NaY and NH_4-USY samples. This is accomplished using a heating rate during the calcination procedure as low as 0.2°C/min. The particle size distribution on the ion-exchanged samples is narrow and the metal is homogeneously distributed throughout the zeolite. With the impregnated zeolite catalysts also a small fraction of larger particles (>2 nm) is found on a part of the zeolite particles. It is also found that preparation of Pt on the mesoporous silica–alumina by impregnation results in <1-nm platinum particles irrespective of the heating rate during the calcination procedure. The need for the extremely low heating rate for the preparation of highly dispersed Pt particles inside zeolite Y is explained by the slow desorption of water and ammonia from the zeolite Y micropores, whereas this process is fast on the mesoporous silica–alumina. In addition, the zeolite micropores might well be able to stabilize mobile Pt species.

EXPERIMENTAL

Catalyst Preparation

In Table 1 are listed the properties of the catalyst supports, and in Table 2 is given a survey of the various catalysts prepared as described below. The catalyst codes contain the procedures used as well as relevant information on the preparation conditions. Also given is the Pt loading as found by atomic absorption spectroscopy or as calculated.

Application of the precursor by ion exchange. Commercial NaY (LZY 54), and NH_4-USY (LZY 84) zeolite powders without binder, obtained from UOP, were used as supports. Some features of the supports are given in Table 1. Note that the information on the USY support is given for the zeolite after desorption of ammonia at 400°C. Whereas the catalyst is prepared by ion exchange of NH_4-USY, this is the composition that is obtained after the preparation procedure (Pt/H-USY). Also, information on the SiO_2–Al_2O_3 (abbreviated as Si–Al) (HA 100 5P, Ketjen) is listed. The aluminum contents (wt%) of the samples are similar and the amorphous silica–alumina has a comparable number of accessible strong Brønsted acid sites per gram as the H-USY support as determined by TPD-TGA of preadsorbed isopropylamine. An important difference is the porous structure of the materials, with only mesopores present in the amorphous silica–alumina and only micropores in the NaY. The H-USY material contains micropores and additionally mesopores. Typically, 10 g of the zeolite powders was suspended in 1 liter water and stirred for 12 h at 70°C. A 0.01 M solution of $Pt(NH_3)_4(NO_3)_2$ (Aldrich 27,872-6 p.a.) was added at the rate of 1.5×10^{-4} mol Pt/h to the support suspension at 70°C with stirring. After addition of the desired amount of precursor solution, the suspension was stirred for another 12 h at 70°C. Subsequently the support was filtered and resuspended in demineralized water at RT to remove nitrate, exchanged cations, and nonexchanged precursor. This procedure (filtering and washing) was repeated two times. Finally, the residues were dried in

TABLE 1

Support Properties

Support	Na (wt%)	$(Si/Al)_{tot}$	Al_F[a] (mmol/g)	Al_{EF} (mmol/g)	Acid sites[b] (mmol/g)	Pores (ml/g)[c] Micro	Pores (ml/g)[c] Meso	S^c_{BET} (m^2/g)
NaY	10	2.5	4.3	0	0	0.34	0.03	(908)
H-USY	0.1	2.5	2.6	2.2	1.4	0.26	0.1	(755)
Si–Al	0[d]	2.5[d]	—[e]	—[e]	1.2	0	0.59	355

[a] F, framework; EF, extraframework.
[b] Determined by TPD-TGA of preadsorbed isopropylamine.
[c] Determined by nitrogen physisorption (T plot, $t = [14.36/(0.1013\text{-}\log(P/P_0)]^{0.5}$ nm).
[d] Determined by ICP. Other data as given by the manufacturer.
[e] ^{27}Al NMR revealed the presence of tetrahedrally and octahedrally coordinated aluminum.

TABLE 2

Catalyst and Pretreatment

Catalyst[a]	Pt (wt%)	Pretreatment[b]	
		Drying[c]	Calcination[d]
Pt/NaY (1.1–IE–no dry, calc)	1.1[e]	—	—
Pt/NaY (1.1–IE–no calc)	1.1[e]	×	—
Pt/NaY (1.1–IE–1)	1.1[e]	×	1°C/min 300°C
Pt/NaY (1.1–IE–0.2)	1.1[e]	×	0.2°C/min 300°C
Pt/NaY (1.1–IE–0.2 water)	1.1[e]	×	+10 vol% water, 0.2°C/min 300°C[g]
Pt/NaY (1.1–IE–0.2 argon)	1.1[e]	×	100% Ar, 0.2°C/min 300°C
Pt/NaY (1.35–IM–0.2)	1.35[f]	×	0.2°C/min 350°C
Pt/H-USY (1.05–IE–no dry, calc)	1.05[e]	—	—
Pt/H-USY (1.05–IE–1)	1.05[e]	×	1°C/min 350°C
Pt/H-USY (1.05–IE–0.2)	1.05[e]	×	0.2°C/min 350°C
Pt/H-USY (1.24–IM–0.2)	1.24[f]	×	0.2°C/min 350°C
Pt/Si–Al (1.5–IM–0.2)	1.5[f]	×	0.2°C/min 300°C
Pt/Si–Al (1.5–IM–1)	1.5[f]	—	1°C/min 300°C
Pt/Si–Al (1.5–IM–5 helium)	1.5[f]	—	100% He, 5°C/min 300°C

[a] Code between brackets; metal loading (wt%)–IE (ion-exchange) or IM (impregnation)–heating rate (°C/min) in calcination.

[b] After calcination all samples were cooled down to RT and reduced in hydrogen 5°C/min to 400°C and kept for 2 h at 400°C.

[c] Samples marked with "×" were predried in argon by heating up with 5°C per minute to 150°C and dried at this temperature overnight.

[d] With 20% O_2 in argon if not specified further.

[e] wt% per gram dry material, determined with AAS.

[f] wt% per gram dry material, calculated by weighing the applied amount of precursors solution.

[g] After calcination the catalyst was dried in inert gas prior to reduction in (dry) hydrogen.

static air at 80°C and stored at RT. The Pt loading of the catalysts was determined (see Table 2) by atomic absorption spectroscopy, using a Varian SpectrAA-400 Zeeman atomic absorption spectrometer, equipped with a graphite tube atomizer.

Application of the precursor by impregnation. The zeolite powder (5 g) was dried in a flask at 150°C in dynamic vacuum for 2 h. After cooling, a solution of $Pt(NH_3)_4(NO_3)_2$ (Aldrich 27,872-6 p.a.) in water was injected into the flask on the dry support in static vacuum. The volume of the injected solution was 90% of the total pore volume of the zeolite supports as determined by nitrogen physisorption (Table 1) (the injected solution for NaY and H-USY was 0.31 and 0.32 ml/g, respectively). The impregnated samples were shaken to ensure a good liquid distribution throughout the support material. Then air was admitted. The impregnated samples were kept at RT for a few hours. The zeolite samples were dried overnight at 80°C in a nitrogen flow in a rotating vaporizer. The Pt metal loadings as calculated from the known volumes and concentrations of precursor solutions are listed in Table 2. Fractionated and sieved amorphous silica alumina (212–425 μm, 5 g) was impregnated with the same procedure except for the predrying at 150°C in dynamic vacuum. This support was only degassed at RT in dynamic vacuum.

Treatments after impregnation and ion exchange. The ion-exchanged and impregnated zeolites were pressed into tablets and then broken and sieved. A sieve fraction of 212–425 μm was collected, the same fraction as with the impregnated amorphous silica–alumina. Samples of typically 0.5–1 g were brought into a fixed bed reactor vertically positioned in an oven. Argon, oxygen, and hydrogen gases were predried on molecular sieve A. High flow conditions were chosen (1 L/min · g) to enhance the desorption rate of water and NH_3 as much as possible and to dilute the desorbing water and NH_3 to diminish their partial pressures. The temperature was measured downstream at the bottom of the fixed bed. In Table 2 the pretreatment procedures for the different catalyst samples are listed. After the drying treatment the calcination was started at 150°C when calcining to 350°C and at 100°C when calcining to 300°C. After the temperature of calcination was reached, the sample was cooled down to RT in argon to flush oxygen if used. Subsequently with all samples the following reduction procedure was executed. In a flow of pure hydrogen the temperature was raised with 5°C per minute to 400°C and kept at this temperature for 2 h. The samples were cooled down in hydrogen and after reaching RT the samples were flushed with argon before admitting air.

Characterization

Hydrogen chemisorption. Chemisorption measurements were performed using a Micromeritics ASAP 2000. Typically, 0.5 g of catalyst was dried in flowing helium at 250°C for 1 h with subsequent evacuation at 50°C for 1 h. The samples were reduced in hydrogen at 400°C for 1 h, cooled down in hydrogen to 200°C, and evacuated for 1 h at this temperature. Subsequently the sample was cooled down *in vacuo* to RT. At 35°C the first isotherm was taken. The H/Pt_{total} ratios (see Table 4 later) are based on the adsorbed amounts of hydrogen determined with this isotherm by extrapolation of the linear part to zero pressure. After the first isotherm was measured, the sample was evacuated at 35°C for 1 h. The second isotherm was obtained. The H/Pt_{strong} ratios (Table 4) are calculated by subtracting the ratios obtained with the second isotherms from the H/Pt_{total} ratios.

EXAFS data collection. The X-ray absorption spectra at the Pt L_3 and L_2 edges were taken at SRS (Daresbury, UK) Wiggler Station 9.2, using a Si(220) double-crystal monochromator. The monochromator was detuned to 50% maximum intensity to avoid higher harmonics present in the X-ray beam. Experiments were also performed at ESRF (Grenoble, France) at BM29, using a Si(311) crystal. The monochromator was detuned to 70% of maximum intensity. Furthermore XAFS data were collected at the HASYLAB (Hamburg, Germany) synchrotron using beamline X1 in transmission mode and a Si(311) crystal. The monochromator was detuned to 50% of maximum intensity. All measurements were done in transmission mode using ion chambers filled with a N_2/Ar mixture to have an X-ray absorbancy of 20% in the first and 80% in the second ion chamber. At the Pt L3 edge (11,564 eV), the estimated resolution was 3 eV for station 9.2 in Daresbury, 1.8 eV for beamline X1 at HASYLAB, and 0.6 eV for beamline BM29 at ESRF. To decrease low- and high-frequency noise as much as possible, an acquisition time of 0.5 s for the EXAFS data was used with a gradual increase to 1.5 s at high electron voltage; three scans were averaged.

The (prereduced) samples were pressed into a self-supporting wafer (calculated to have an absorbance of 2.5) and placed in a controlled-atmosphere cell operated at 1 atm (16). Subsequently, the catalysts were dried at 150°C for 2 h, rereduced in pure hydrogen flow at 400°C, and cooled down in hydrogen flow to RT. Then the hydrogen supply was disconnected from the cell and the cell was cooled down to liquid nitrogen temperature.

EXAFS data analysis. Standard procedures were used to extract the EXAFS data from the measured absorption spectra (17). Normalization was done by dividing the absorption intensities by the height of the absorption edge and subtracting the background using cubic spline routines. The final EXAFS function was obtained by averaging three individual background-subtracted and normalized EXAFS data.

Data analysis was performed by multiple shell fitting in R space. Backscatterers Pt and O were identified by applying the difference file technique using phase-corrected Fourier transforms (18). Data for the phase shifts and backscattering amplitudes were obtained from FEFF7 calculations (19).

TEM. (Pre)reduced catalysts, stored under air, were suspended in ethanol and ultrasonically dispersed. Drops of the dispersions were applied on a copper grid-supported carbon film. A Philips EM420 transmission electron microscope, operated at 120 kV, was used to investigate the samples. Transmission electron micrographs were recorded at a magnification of 54,000.

XRD. Powder X-Ray diffraction measurements were carried out with a Nonius PDS diffractometer system, equipped with a position-sensitive detector of 120 2θ. The radiation used was Cu$K\alpha_1$. The average Pt crystal size was calculated with the Scherrer equation.

Combination of TEM, EXAFS and Particle Modelling

EXAFS analysis renders an average first-shell coordination number $N_{\mathrm{Pt-Pt}}$ for all platinum atoms in the zeolite Y crystals. This number can be related to the complete particle size distribution, $P/g_{\mathrm{zeolite}}(\mathrm{size})$, defined as the number of platinum particles per size per gram catalyst: $P/g_{\mathrm{zeolite}}(\mathrm{size})$:

$$N_{\mathrm{Pt-Pt}} = \frac{\mathrm{MW_{Pt}}}{N_{\mathrm{Av}} * \mathrm{Pt_{loading}}} \int_{\mathrm{size}=0}^{\infty} P/g_{\mathrm{zeolite}}(\mathrm{size}) * A(\mathrm{size}) * N_{\mathrm{Pt-Pt}}(\mathrm{size})\, d\ \mathrm{size}, \quad [1]$$

where

$\mathrm{MW_{Pt}}$ = molecular weight of platinum (g/mol),
N_{Av} = Avogadro's number,
$\mathrm{Pt_{loading}}$ = weight of platinum per weight of zeolite (g Pt/g zeolite),
$A(\mathrm{size})$ = number of platinum atoms per particle size,
$N_{\mathrm{Pt-Pt}}(size)$ = first-shell coordination number of platinum particles per size.

Another technique that provides information on particle size distribution is hydrogen chemisorption. The calculated H/Pt value from hydrogen chemisorption experiments can be related to the complete particle size distribution when (also) the fraction of surface atoms per particle size (dispersion) $D(\mathrm{size})$ is known:

$$\mathrm{H/Pt} = \frac{\mathrm{MW_{Pt}}}{N_{\mathrm{Av}} * \mathrm{Pt_{loading}}} \int_{\mathrm{size}=0}^{\infty} P/g_{\ \mathrm{zeolite}}(\mathrm{size}) * A(\mathrm{size}) * D(\mathrm{size})\, d\ \mathrm{size}. \quad [2]$$

Difficulty in this approach lies in the adsorption stoichiometry of hydrogen on platinum. The presented equation is valid only when this number is 1.

To use Eqs. [1] and [2] information about $A(\mathrm{size})$, $N_{\mathrm{Pt-Pt}}(\mathrm{size})$, and $D(\mathrm{size})$ has to be obtained. Spherically shaped platinum particles were modeled assuming a face-centred cubic structure for platinum in the particles in the size range 6 to 1000 atoms per particle using a computer program (20). The number of atoms per size, $A(\mathrm{size})$, was calculated taking the diameter of the modeled particles as the size. The first-shell coordination number per size, $N_{\mathrm{Pt-Pt}}(\mathrm{size})$, was calculated by numerically averaging over all coordinations present in the individual modeled particles. The number of surface atoms per particle, $D(\mathrm{size})$, was calculated using the definition of surface atoms having

less than 12 neighboring atoms. The size range of these functions was expanded to 250 nm (>50,000 atoms per particle) by extrapolation.

TEM analysis on Pt/Y has as a lower detection limit of platinum particles around a few nanometers. By combining TEM, EXAFS, and particle modeling the (volume) average size of the platinum particles that are not visible with TEM can be determined. The part of the particle size distribution visible by TEM is obtained by counting the number of projected platinum particles per size per area of zeolite crystal. The number of platinum particles per volume is estimated on basis of the assumptions that the zeolite crystals do have equal dimensions in all directions, and that the platinum particles in this zeolite volume are projected and distinguishable in the transmission electron micrograph. Using these results and the density of the zeolite particles, the part of the particle size distribution visible by TEM can be obtained.

After integration of Eq. [1] by using the part of the platinum particle size distribution detected with TEM as described above and the established Pt loading, the following equation is obtained:

$$N_{\text{Pt–Pt}} = N_{\text{Pt–Pt, not detected with TEM}} * (1 - \text{mass fraction}_{\text{TEM}}) + N_{\text{Pt–PtTEM}} * \text{mass fraction}_{\text{TEM}}, \quad [3]$$

where mass fraction$_{\text{TEM}}$ = fraction of Pt metal that is detected with TEM. From this equation $N_{\text{Pt–Pt not detected with TEM}}$ can be obtained. There the mass fraction of the particles in the size distribution as determined with TEM is calculated by estimating the mass of the particles using their size and the modeled atom size function, A(size). The (average) coordination number of the particles in the size distribution as determined with TEM is calculated by using their size and the modeled first-shell coordination number size function, $N_{\text{Pt–Pt}}$(size). With the thus calculated $N_{\text{Pt–Pt not detected with TEM}}$ the volume average particle size of the corresponding platinum particles is estimated with the modeled first-shell coordination number size function, $N_{\text{Pt–Pt}}$(size).

The results obtained with hydrogen chemisorption are compared with the results calculated as described above to check the applied procedure.

RESULTS

Preparation of Zeolite-Supported Pt Catalysts

Table 2 gives an overview of the different zeolite-supported Pt catalysts. As supports NaY, H-USY, and amorphous SiO_2–Al_2O_3 were used. Both ion exchange and impregnation with $Pt(NH_3)_4(NO_3)_2$ as precursor were applied. The Pt metal loading is around 1 wt% for all samples. Different gases were applied during the calcination procedure (Ar, He, O_2, O_2/H_2O). The heating rate during the calcination procedure is varied from 1°C/min (as normally used in the literature) to a much lower value of 0.2°C/min. After calcination all samples were cooled down to RT and reduced in hydrogen at 400°C using a heating rate of 5°C/min.

EXAFS Data Analysis and Results

In Fig. 1A the experimental k^2-weighted EXAFS function of catalyst Pt/NaY(1.1–IE–0.2) is plotted. The quality of the data is representative of all experiments. Figure 1B shows that the imaginary part and absolute part of the Fourier transform of the fit and the experimental data fit very well between 1.6 and 3.1 Å. In Table 3 the fit parameters of the EXAFS data analysis are listed. For all samples the variance of the fit of the imaginary part and absolute part of the Fourier transform is less than 1%,

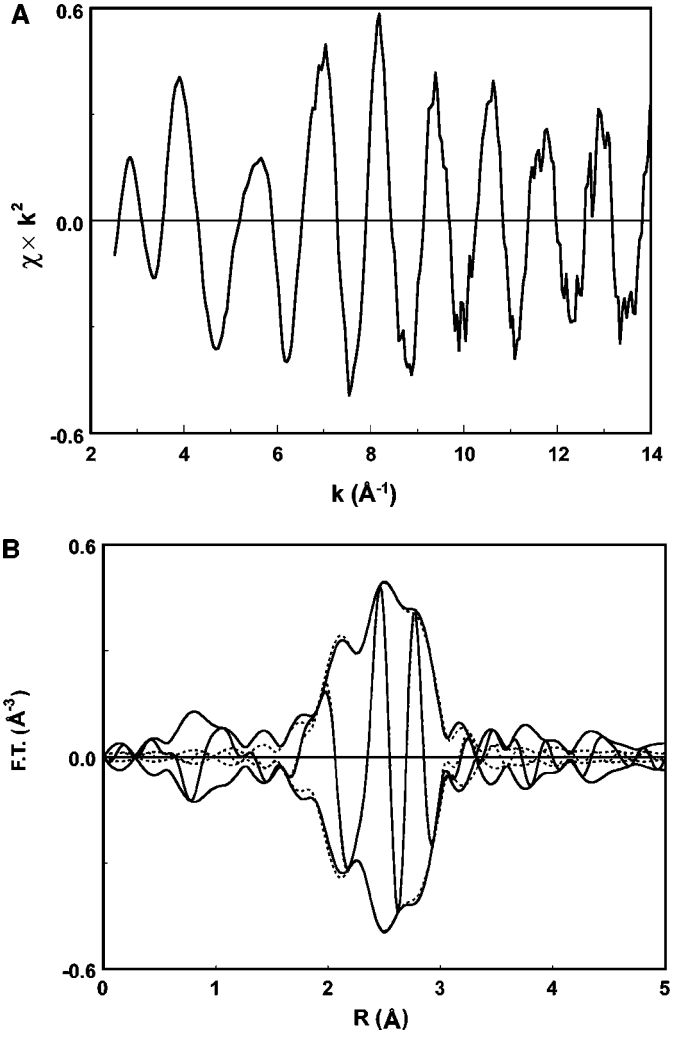

FIG. 1. (A) Experimental k^2-weighted EXAFS spectrum for Pt/NaY (1.1–IE–0.2); (B) Fourier transform (k^2-weighted, Δk 2.5–14 Å^{-1}) of experimental data (solid line) and total (Pt–Pt + Pt–O) fit (dotted line).

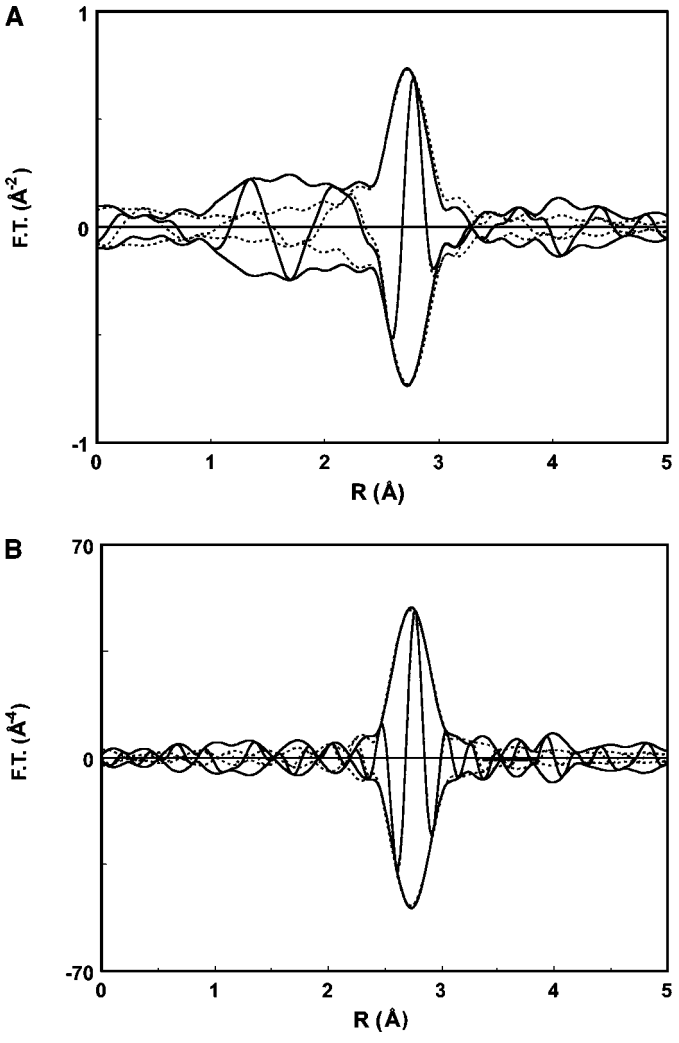

FIG. 2. (A) Fourier transform (k^1-weighted, Δk 3.5–14 Å^{-1}, Pt–Pt phase, and amplitude corrected) of difference file (raw EXAFS data minus Pt–O-fitted contribution) (solid line) and Pt–Pt fitted contribution (dotted line) for Pt/NaY(1.1–IE–0.2). (B) Fourier transform (k^3-weighted, Δk 3.5–14 Å^{-1}, Pt–Pt phase, and amplitude corrected) of difference file (raw EXAFS data minus Pt–O fitted contribution) (solid line) and Pt–Pt fitted contribution (dotted line) for Pt/NaY (1.1–IE–0.2).

indicating a high-quality fit. Moreover Fig. 2A and 2B show that the Fourier transform of the fitted Pt–Pt contribution agrees very well with the Fourier transform of the corresponding difference file (experimental EXAFS minus Pt–O contribution) in both k^1 and k^3 weighting, indicating a reliable decoupling of the Pt–Pt coordination number and the Debye–Waller factor (18). The k^1-weighted Fourier transform (FT) of the fitted Pt–O oxygen contribution and the FT of the corresponding difference file (experimental EXAFS minus the fitted Pt contribution) are displayed in Fig. 3. The Fourier transform of the Pt–O contribution approximates very well the Pt–O peak in the FT of the difference file. Figure 3 shows also the atomic XAFS (AXAFS) peak around a distance of 1.2 Å. This peak is due to scattering of the outgoing electron against the deep valence electrons of the X-ray-absorbing atom. The intensity of the FT AXAFS peak has been found to depend on the acidity/alkalinity of the support, and has been proven to be a promising tool in the study of metal–support effects (21).

The first-shell platinum coordination number, $N_{\text{Pt–Pt}}$, (Table 3), appears strongly dependent on the treatment applied to the Pt/NaY catalysts. When calcination is omitted, a high platinum coordination number is found, indicating the presence of large platinum particles. When calcination is included in the procedure the platinum coordination number is much lower. Furthermore the heating rate used during calcination has a pronounced effect on the $N_{\text{Pt–Pt}}$ coordination number; the lowest numbers, i.e., the smallest platinum particles, are found when using a heating rate of 0.2°C, with both ion-exchanged Pt/NaY and Pt/H-USY. This calcination procedure results in slightly larger $N_{\text{Pt–Pt}}$ values on the impregnated zeolite catalysts, whereas the coordination number on the impregnated silica–alumina is similar that of the ion-exchanged zeolites. With all catalysts in this study, zeolite supported and silica-alumina supported Pt–O contributions are found at a distance of 2.6 Å.

Hydrogen Chemisorption

Table 4 lists the H/Pt ratios determined for the various catalysts. Both the ratios obtained in the first isotherm, H/Pt_{total}, and the ratios obtained after subtraction of the amount of removable hydrogen at 35°C, H/Pt_{strong}, vary significantly. However, the H/Pt_{total} ratio is for each catalyst about twice as high as the H/Pt_{strong} ratio, which shows that the correlation with Pt surface area is the same for both

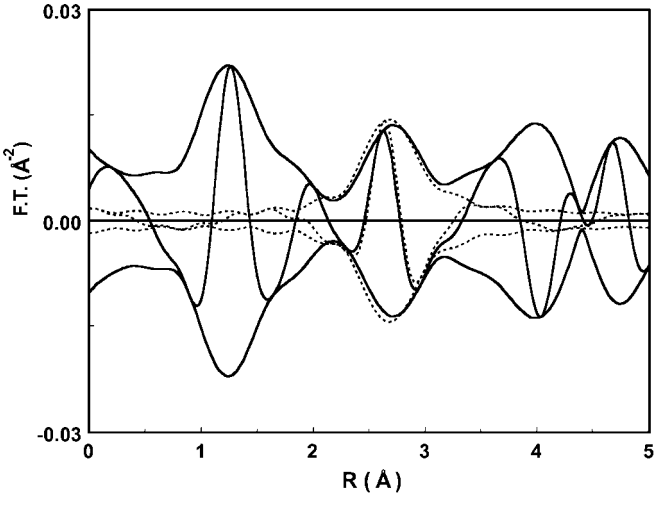

FIG. 3. Fourier transform (k^1-weighted, Δk 2.5–10 Å^{-1}, Pt–O phase corrected) of difference file (raw EXAFS data minus Pt–Pt fitted contribution) (solid line) and Pt–O fitted contribution (dotted line) for Pt/NaY (1.1–IE–0.2).

TABLE 3

Fit Parameters of EXAFS Spectra and Variances of Fits ($\Delta k = 2.5$–14 Å^{-1}, $\Delta R = 1.6$–3.1 Å, k^2 Weighted)

Catalyst	Scatterer	N ±10%	R (Å) ±1%	$\Delta\sigma^2$ (10^{-3} Å^2) ±5%	ΔE_0 (eV) ±10%	k^2 variance (%) Im.	Abs.
Pt/NaY (1.1–IE–no dry, calc)	Pt	11.2	2.76	−0.02	0.29	0.24	0.15
	O	0.7	2.62	10	−5.71		
Pt/NaY (1.1–IE–no calc)	Pt	10.1	2.75	2.65	0.43	0.15	0.07
	O	0.6	2.65	10	−2.38		
Pt/NaY (1.1–IE–1)	Pt	6.9	2.75	1.91	2.26	0.32	0.19
	O	0.9	2.62	4.78	2.10		
Pt/NaY (1.1–IE–0.2)	Pt	5.4	2.75	4.28	3.33	0.31	0.15
	O	0.4	2.65	−1.65	−2.96		
Pt/NaY (1.35–IM–0.2)	Pt	6.1	2.75	3.19	2.00	0.53	0.20
	O	0.5	2.66	10	0.28		
Pt/H-USY (1.05–IE–1)	Pt	7.8	2.76	0.96	1.65	0.15	0.05
	O	1.1	2.58	8.82	3.02		
Pt/H-USY (1.05–IE–0.2)	Pt	5.6	2.76	2.23	1.85	0.73	0.37
	O	1.1	2.65	10.84	1.17		
Pt/H-USY (1.24–IM–0.2)	Pt	6.3	2.76	2.63	0.70	0.41	0.27
	O	0.8	2.67	10	0.29		
Pt/Si-Al (1.5–IM–1)	Pt	5.3	2.76	3.21	1.18	0.22	0.13
	O	1.5	2.61	13.18	5.53		

numbers. According to conventional use, the catalysts are compared on the basis of H/Pt_{strong} ratios.

For the ion-exchanged zeolites this ratio is found to depend strongly on the treatment conditions. The highest number (1.2–1.0) is found when the zeolites are calcined at a heating rate of 0.2°C per minute, whereas a heating rate of 1°C per minute results in a substantially lower value. The H/Pt_{strong} ratio of impregnated zeolite calcined at 0.2°C per minute is 0.45–0.5. With silica–alumina as the support similar values (0.56–0.58) are obtained irrespective of the calcination/precursor decomposition procedure.

Although quantification of the platinum surface sites on the basis of hydrogen chemisorption results is controversial, the observed difference in H/Pt ratio for different catalysts based on the same support must be due to a difference in dispersion.

TABLE 4

Results of Catalyst Characterization

Catalyst	H/Pt Total	H/Pt Strong	N_{Pt-Pt}	TEM
Pt/NaY (1.1–IE–no dry, calc)	0.1	<0.1[b]	11.2	20–40 nm (⟨25 nm⟩[c])
Pt/NaY (1.1–IE–no calc)	n.d	n.d.	10.1	n.d
Pt/NaY (1.1–IE–1)	1.0	0.44	6.9	5%[a] 4–9 nm, 95%[a] <2 nm
Pt/NaY (1.1–IE–0.2)	2.1	1.2	5.4	<2 nm
Pt/NaY (1.1–IE–0.2 water)	n.d	n.d.	n.d	>10%[a] 4–9 nm
Pt/NaY (1.1–IE–0.2 argon)	1.5	0.77	n.d.	<5%[a] 5 nm
Pt/NaY (1.35–IM–0.2)	1.1	0.50	6.1	Occasionally >2 nm
Pt/H-USY (1.05–IE–no dry)	0.1	<0.1[c]	n.d.	n.d.
Pt/H-USY (1.05–IE–1)	0.9	0.3	7.8	8%[a] 4–9 nm, 92%[a] <2 nm
Pt/H-USY (1.05–IE–0.2)	2.0	1.0	5.6	<2 nm
Pt/H-USY (1.24–IM–0.2)	1.1	0.45	6.3	Occasionally >2 nm
Pt/Si-Al (1.5–IM–0.2)	1.1	0.58	n.d.	n.d.
Pt/Si-Al (1.5–IM–1)	1.1	0.56	5.3	<2 nm
Pt/Si-Al (1.5–IM–5 helium)	1.1	0.58	n.d.	<2 nm

[a] Amounts in percent of applied loading.
[b] Inaccuracy is high.
[c] Average diameter of 25 nm was determined with XRD.

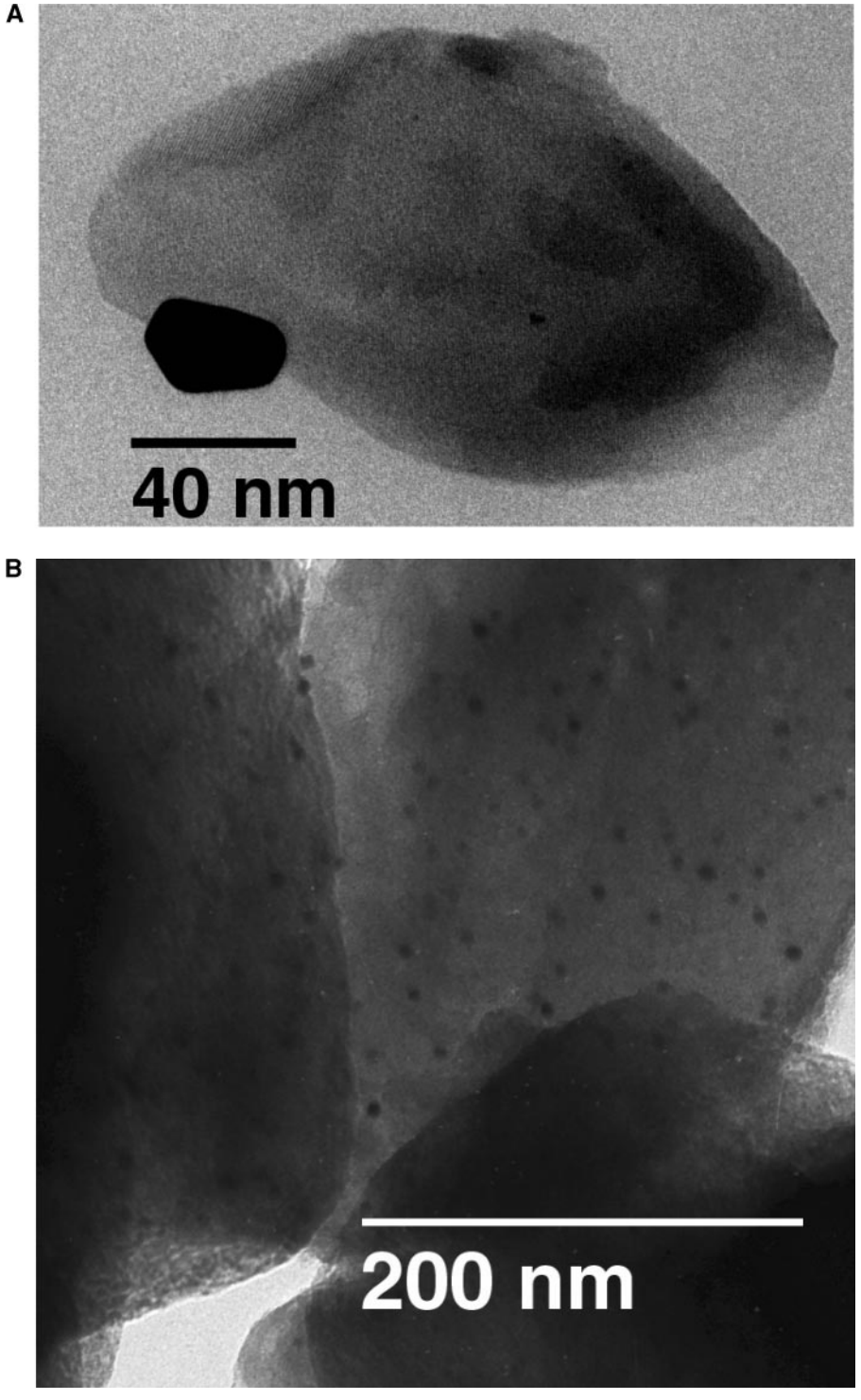

FIG. 4. (A) TEM of Pt/NaY (1.1–IE–no dry, calc), showing a large platinum crystallite on the exterior of the zeolite particle. (B) TEM of Pt/NaY (1.1–IE–1), showing platinum particles in the size range 4–9 nm occluded in the zeolite with a few on the exterior of the zeolite particles. (C) Thin zeolite particle of sample Pt/NaY (1.1–IE–1), showing platinum particles of a size of about 6 nm occluded in the zeolite particle.

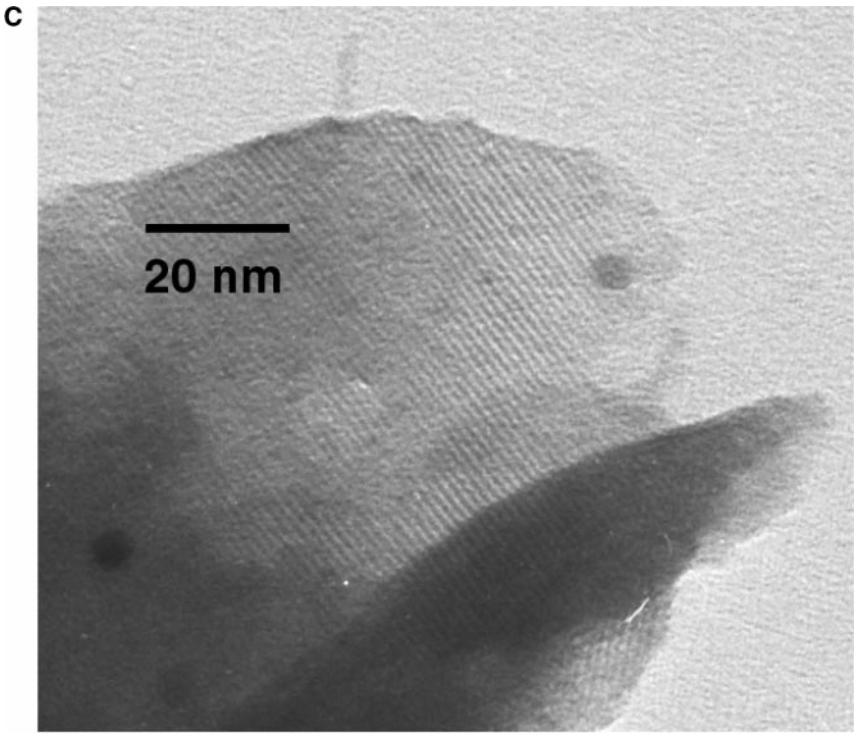

FIG. 4—*Continued*

TEM

Very large platinum particles (Fig. 4A) were observed at the exterior of the ion-exchanged zeolite crystals when the catalysts had not been calcined before reduction. When the ion-exchanged zeolite samples had been calcined at a heating rate of 1°C/min prior to reduction, platinum particles were observed in the size range 4–9 nm (partially) occluded in the internal structure of the zeolite crystals (Figs. 4B, 4C). No platinum particles larger than 2 nm were observed on the ion-exchanged zeolites that had been calcined at 0.2°C/min. On the impregnated and 0.2°C/min calcined zeolite catalysts occasionally larger platinum particles (>2 nm) were observed on a part of the zeolite particles. TEM analysis of the Pt on silica–alumina catalyst showed the platinum to be well dispersed irrespective of the heating rate used during calcination. The transmission electron micrographs of Pt/NaY (1.1–IE–1) and Pt/H-USY(1.05–IE–1) were analyzed as described under Experimental and the P(size) distributions are given in Figs. 5A and 5B. These distributions show that the average size of the Pt particles of the Pt/H-USY catalyst is higher than that of the Pt/NaY catalyst. Moreover, the number of particles per gram of Pt/H-USY is higher than that per gram of Pt/NaY.

XRD

Only with the catalysts that had not been calcined before reduction was platinum detected by powder

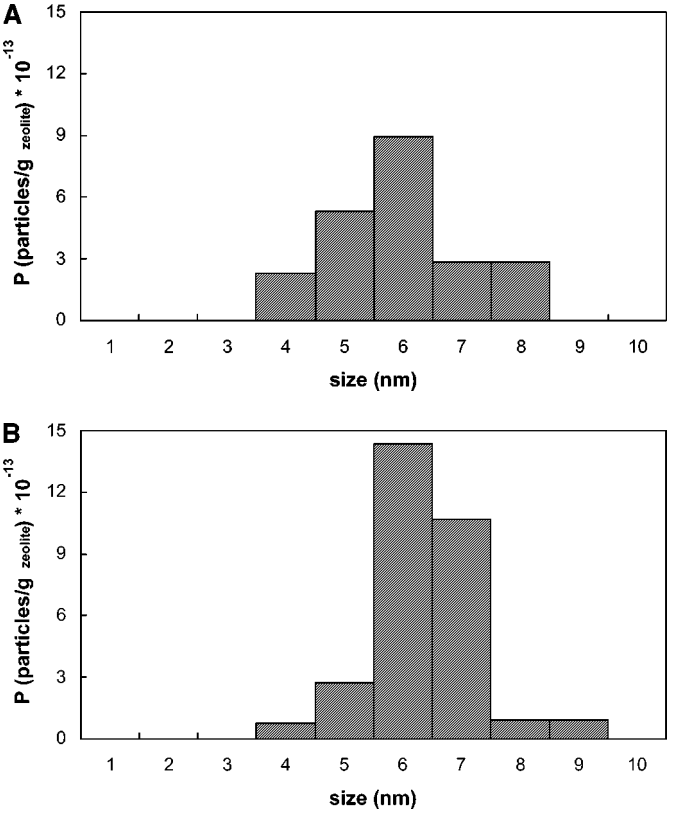

FIG. 5. (A) Particle size distribution, P(size), of catalyst Pt/NaY (1.1–IE–1). (B) Particle size distribution, P(size), of catalyst Pt/HUSY (1.05–IE–1).

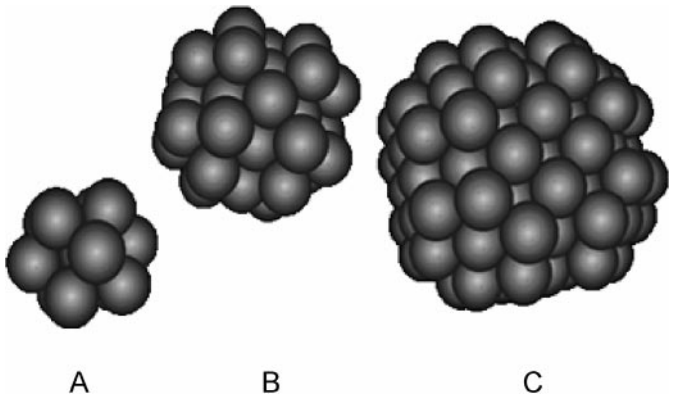

FIG. 6. Examples of modeling Pt particles. (A) 13 atoms; N_{Pt-Pt} = 5.54; dispersion = 0.92; fits in sphere of 8.3 Å. (B) 43 atoms; N_{Pt-Pt} = 7.26; dispersion = 0.98; fits in sphere of 12.8 Å. (C) 135 atoms, N_{Pt-Pt} = 8.89; dispersion = 0.68; fits in sphere of 17.8 Å.

diffraction. From the line broadening of the Pt(111) diffraction an average crystal size of 25 nm was calculated for Pt/NaY(1.1–IE–no dry, calc). Whereas the absence of the Pt pattern is expected for highly dispersed platinum, with samples containing platinum particles of 6–10 nm this must be due to the low abundance of platinum in this size range (only 0.05–0.08 wt%).

Particle Modeling

Figure 6 shows the results of the particle modeling. The number of atoms per particle per size, A(size), is plotted in the ranges 0.5–2 and 0–25 nm in Figs. 7A and 7B, respectively. The first-shell coordination number N_{Pt-Pt}(size) is plotted in Fig. 8 in the size range 0–25 nm. Figure 9 shows the calculated dispersion D(size) as a function of the particle size.

DISCUSSION

Platinum Particle Size Distribution from TEM, EXAFS, and Hydrogen Chemisorption

The experimental results obtained with hydrogen chemisorption, EXAFS, and TEM analysis (see Table 4) and the modeling results for A(size) (Figs. 7A and 7B), N_{Pt-Pt}(size) (Fig. 8), and D(size) (Fig. 9) were used to calculate the average particle size and the average number of atoms per particle for a few selected samples.

For the catalysts for which TEM did not reveal or hardly revealed the presence of large platinum particles (4–9 nm) (Pt/NaY), this calculation was done by combining the experimental EXAFS N_{Pt-Pt} numbers (Table 4) with the N_{Pt-Pt} (size) function (Fig. 8) and the A(size) function (Fig. 7A). The results are presented in Table 5.

For the zeolite catalysts calcined at 1°C/min TEM revealed the presence of large particles. The mass fraction$_{TEM}$ of the particles in the size distribution as determined by TEM is calculated by estimating the mass of the particles

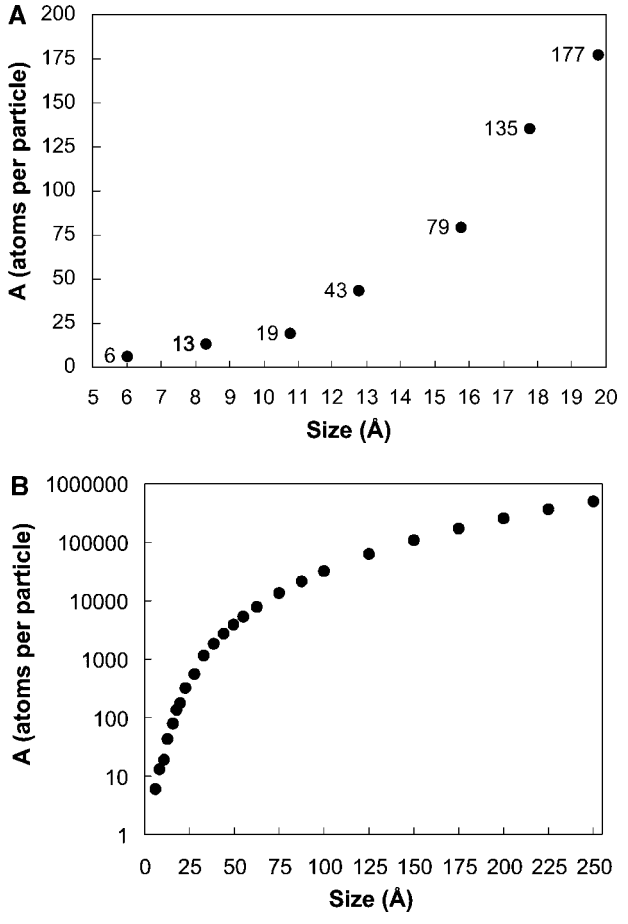

FIG. 7. Numbers of atoms per modeled particle in the size ranges (A) 0.5–2 nm and (B) 0.5–25 nm. The number of atoms per particle in A is plotted next to the data. Y scale is logarithmic.

using their size and the modeled atom size function, A(size). From the particle size distributions (Figs. 5A, 5B), applied loading, and relation between the first-shell coordination number and particle size (Fig. 8), the average coordination

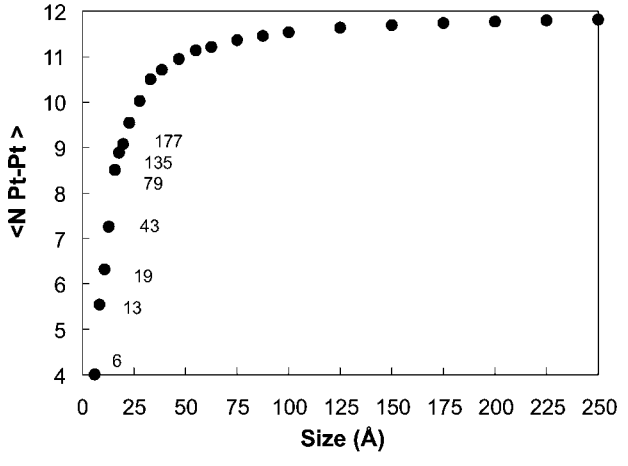

FIG. 8. First-shell coordination number N_{Pt-Pt} per modeled particle in the size range 0.5–25 nm. The number of atoms per particle is plotted next to the data in the size range 0.5–2 nm.

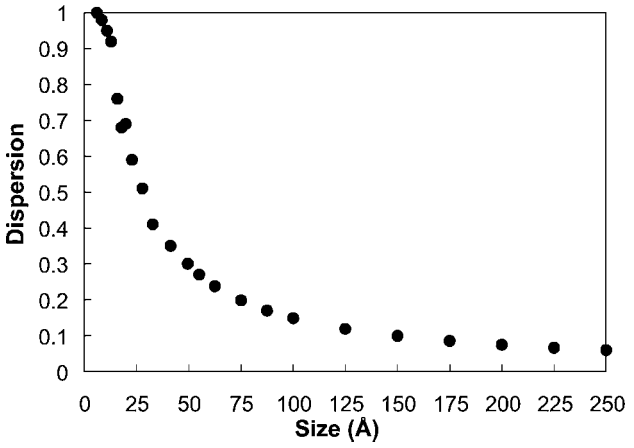

FIG. 9. Dispersion (atoms with coordination less than 12 divided by atoms with coordination 12) per modeled particle in the size range 0–25 nm. Note: The discontinuity in the function at low particle size is real and is due to addition of a full shell of atoms to very small particles, which has a large effect on the dispersion.

number of the particles observed by TEM ($N_{\text{Pt–Pt TEM}}$) for both catalysts is calculated to be 11.3. With this number and using Eq. [3], the average coordination number of the mass fraction of platinum particles of catalyst Pt/NaY (1.1–IE–1) <2 nm ($N_{\text{Pt–Pt not detected with TEM}}$) is found to be 6.7 [(1/0.95) × (6.9–0.05 × 11.3)], and for catalyst Pt/H-USY(1.05–IE–1) this coordination number is found to be 7.5 [(1/0.92) × (7.8-0.08 × 11.3)]. The corresponding average size and number of atoms per particle as given in Table 5 were calculated by combining these calculated coordination numbers with the $N_{\text{Pt–Pt}}$ (size) function (Fig. 8) and the A(size) function (Fig. 7A) derived from the modeled particles.

The accuracy of the EXAFS coordination numbers used to calculate the average particle size is 10%. This statistical error is included in the sizes listed in Table 5. The weight factor in the averaging of the coordination number over all particles is the fraction of platinum atoms of a given coordination. Because the number of atoms per particle increases with approximately r^3 and the coordination number of the particles strongly depends on their size (Fig. 8), the larger particles in a size distribution dominate the average EXAFS coordination number. The deduced average particle size from EXAFS analysis of a (narrow) particle size distribution is therefore a volume average of the particle size distribution and an overestimation of the diameter average of the particle size distribution. On the other hand TEM cannot be used to detect Pt particles smaller than 2 nm. A combination of TEM and EXAFS is a powerful method to detect bimodal particle size distributions. A schematic presentation is given in Fig. 10 of the size range (nm/number of atoms per particle) where EXAFS and TEM have to be used to determine particle size accurately.

The largest error in the analysis of transmission electron micrographs is beyond doubt introduced by the limited number of TEM projections that are analyzed and assumed to be representative. Samples used for TEM had been exposed to air. EXAFS analysis revealed that platinum particles of about 1 nm are completely oxidized under these conditions, whereas particles of a few nanometers are only partially oxidized. Because with TEM analysis no discrimination can be made between the oxidic and metallic state, and the mass of the particles is calculated using their sizes, an error is introduced because of the unknown platinum atom density. As the observed platinum particles are assumed metallic, this error is an overestimation of the platinum mass of maximal 30% when the actual particles would be completely oxidized (22, Table 6). In fact for the analysis of particles in the range 4–9 nm this potential error will be insignificant because in this size range only surface oxide is formed.

The modeling of the size functions is based on spherically shaped particles. The shape of the particle determines the relation between the number of surface atoms (dispersion) and their average coordination number ($N_{\text{Pt–Pt}}$). The 2D

TABLE 5

Calculated Particle Size Distribution

Catalyst	Particles <2 nm: Average size	Particles <2 nm: Atoms per particle	Particles >2 nm
Pt/NaY (1.1–IE–1)	95%[a] 1–1.1 nm	30 ± 10	5%[a] 4–9 nm
Pt/NaY (1.1–IE–0.2)	<0.9 nm	13 ± 5	—
Pt/NaY (1.35–IM–0.2)	1–1.1 nm	20 ± 5	Occasionally
Pt/H-USY (1.05–IE–1)	92%[a] 1–1.2 nm	45 ± 15	8%[a] 4–9 nm
Pt/H-USY (1.05–IE–0.2)	<0.9 nm	13 ± 5	—
Pt/H-USY (1.24–IM–0.2)	1–1.1 nm	20 ± 5	Occasionally
Pt/Si–Al (1.5–IM–1)	<0.9 nm	13 ± 5	—

[a] % of applied loading.

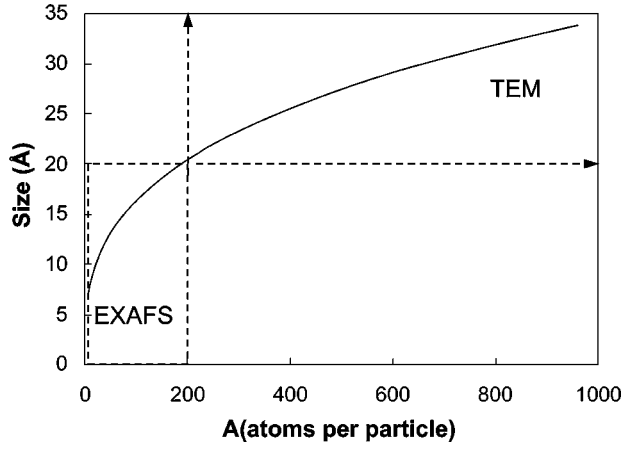

FIG. 10. Schematic presentation of the size range/number of atoms per particle where EXAFS and TEM are used to determine the particle size accurately.

TEM projections of catalysts calcined at 1°C/min (Figs. 5A, 5B) show the 4- to 9-nm particles (partially) occluded in the zeolite to have a spherical shape. By using HRTEM a spherical shape was found for small platinum particles dispersed in zeolite Y of a size 1–2 nm also (14). The stability of noble metal particles is driven largely by maximization of the average coordination number of the atoms. This implies for very small particles (below 1 nm) the formation of spherical shapes, as shown with embedded atomic modeling (23). In the case of (strong) metal–support interaction the formation of raft-like particles has been reported (3). For Pt on Al_2O_3 this is observed after reduction at 450°C. EXAFS analysis revealed a short Pt–O distance of 2.2 Å on this catalyst. Three–dimensional particles are formed by reduction at lower temperature and then a Pt–O distance of 2.7 Å is observed (24). For all catalysts investigated in this paper a Pt–O distance of 2.6 Å was found (Table 3). Obviously zeolite Y has a tendency to preserve three-dimensional metal particles within its spherical shaped micropores (24).

To estimate the reliability of the procedure of combining TEM and EXAFS results and the modeled size functions, the calculated particle sizes are correlated with the H/Pt values as determined from the hydrogen chemisorption results. TEM and EXAFS analysis on catalyst Pt/NaY(1.1–IE–1) revealed 5% of the metal to be present as 4- to 9-nm particles with an average calculated coordination number of 6.7 for the other 95%. With this catalyst a H/Pt_{strong} value of 0.44 is found (Table 4). Suppose the TEM analysis failed and the actual mass percentage of metal as 4- to 9-nm particles had been 25% instead of 5%. In that case, using the EXAFS coordination number for this catalyst and Eq. [3], the remaining 75% of the metal should have been particles with an average coordination number of 5.4. With such small particles, a high chemisorption of hydrogen is expected: for instance with catalyst Pt/NaY(1.1–IE–0.2) an H/Pt_{strong} value of 1.2 and an average coordination number of 5.4 were found. The dispersion of particles in the size range 4–9 nm is about 0.2 (Fig. 9). Hence, if the actual mass percentage of metal in the size range 4–9 nm on Pt/NaY(1.1–IE–1) had been 25% instead of 5% as supposed above, the expected H/Pt_{strong} value should have been 0.92 $[0.75 \times 1.2 + 0.25 \times 0.2 \times 0.44]$ and not the obtained value of 0.44. Similar reasoning holds for the Pt/H-USY(1.05–IE–0.2) catalysts. From these results it can be concluded that the hydrogen chemisorption data support the followed procedure of combining TEM, EXAFS, and particle modeling.

The supercages in zeolite Y are spherical with a diameter of 1.2 nm and therefore large enough to accommodate the small particles obtained after ion exchange and calcination at a heating rate as low as 0.2°C per minute, i.e., with Pt/NaY(1.1–IE–0.2) and Pt/H-USY(1.05–IE–0.2). Calcination with heating rates even as low as 1°C/min leads to a bimodal platinum particle size distribution for ion-exchanged zeolite catalysts. A minority (5 and 8%) of large particles (4–9 nm) do not fit in the micropores and are localized at the outside of the zeolite crystal or are occluded in the zeolite crystals which must result in local destruction of the framework. Calcination of impregnated zeolite at 0.2°C per minute leads to platinum particles not that homogeneously distributed as with ion exchange, with a small fraction larger than 2 nm. However, the average Pt particle size is still 1–1.1 nm or 20 atoms. On the other hand, calcination of impregnated silica–alumina catalysts at a heating rate of 1°C per minute resulted in a homogeneous Pt particle size distribution similar to that observed with the ion-exchanged zeolites calcined at 0.2°C per minute.

The H/Pt adsorption ratios (Table 4) deviate largely for $Pt/SiO_2–Al_2O_3$(1.5–IM–1) and both Pt/NaY(1.1–IE–0.2) and Pt/H-USY(1.1–IE–0.2). These catalysts comprise exclusively Pt particles smaller than 2 nm whereas the H/Pt_{strong} ratios are 0.56–0.58, 1.2, and 1.0, respectively. To our knowledge no fundamental explanation has been given for this phenomenon. Possibly, adsorbed hydrogen is stabilized by both Pt and the zeolite cavity walls, thereby enhancing H/Pt ratios for zeolite-supported catalysts.

Evaluation of Preparation Procedures with $Pt(NH_3)_4^{2+}$ Ion-Exchanged Zeolite Y

Direct reduction of the ammonia coordinated precursor, $Pt(NH_3)_4^{2+}$. The shortest route leading to metallic platinum is direct reduction with hydrogen of the $Pt(NH_3)_4^{2+}$ ion-exchanged zeolite. However, this results in poor metal dispersions (3) as shown in Table 4 (Pt/NaY, Pt/H-USY(1.05–IE–no dry, calc). Although the precursor is ion-exchanged on cation sites inside the supercages of the zeolite crystals, large metal particles are formed at the exterior of the zeolite crystals (Fig. 4). Direct reduction of ion-exchanged zeolite dried at 150°C still results in a low metal dispersion (Table 4, Pt/NaY(1.1–IE–no calc). With TPR the onset temperature of reduction was found to be 150°C at which temperature a change in color from white to gray occurs. The desorption of ammonia from the $Pt(NH_3)_4^{2+}$ ion, exchanged in zeolite Y, is known to occur between 200 and 300°C (25). This means that at the onset of the reduction ammonia ligands are still coordinated to the platinum cations. Apparently ammonia ligands coordinated to the platinum cations prevent the formation of small (and stable) metallic particles inside the zeolite. An explanation for this is the formation of mobile neutral platinum ammonia hydride, $Pt^0(NH_3)_2H_2$ (3). The reason that large Pt particles are formed at the exterior of the zeolite can now be explained. At the exterior of the zeolite particles the ammonia partial pressure is low due to fast desorption from the zeolite surface and dilution by the external gas flow. As a result stable metallic particles are formed that grow due to

deposition–reduction of mobile precursor species migrating out of the micropores. In line with the literature (3, 7–9) it is concluded that ammonia must be removed prior to reduction of the ion-exchanged zeolite to obtain small platinum particles in the micropores.

Reduction of the calcined precursor. To remove ammonia from the precursor before reduction in hydrogen, calcination of the ion-exchanged zeolite NaY to 300°C has been recommended (26). At this temperature the calcined precursor is reported to remain in the supercage structure of the zeolite. Calcination of the ion-exchanged zeolite at 500–600°C results in migration of the calcined precursor to sodalite cages. This precursor can be reduced only at high temperature. The resulting dispersion is then low (4, 27). To remove ammonia from the acid sites of the ion-exchanged NH_4-USY support the calcination was performed to a temperature of 350°C instead of 300°C on this catalyst precursor.

The metal dispersion after reduction of the calcined ion-exchanged zeolite turned out to be much higher than when the ammonia coordinated precursor had been directly reduced in hydrogen. The metal dispersion was even higher when a heating rate of 0.2°C instead of 1°C per minute was used (Table 4). The crucial parameter is the heating rate and not the calcination time, as heating ion-exchanged zeolite Y at 1°C/min to 300–350°C and further calcination at these temperatures for hours did not result in an improved Pt dispersion. This sensitivity of the dispersion to the heating rate was reported earlier (8) and can be explained as follows.

The reduction conditions as applied in this study are kept the same for the preparation of all catalysts. Apparently, the dispersion of the calcined precursor is key to the final dispersion of the Pt metal particles. Initially, the precursor is ionically dispersed, and most likely statistically distributed through the supercages of the Y crystals. During calcination the ammonia ligands are removed from the $Pt(NH_3)_4^{2+}$ ions and are oxidized to N_2O and water (8).

The classic explanation for the sensitivity of the final metal dispersion to the heating rate is the uncompleted oxidation of ammonia when heating up too fast, leading to autoreduction of the Pt precursor. This process is known to occur on heating to 300°C in inert atmospheres and as a result less well dispersed platinum has been obtained (7) in agreement with the lower H/Pt ratio on Pt/NaY(1.1–IE–0.2 argon) than on the catalyst that was calcined in 20% oxygen in argon. Heating at 0.2°C per minute means more time to remove ammonia by oxidation and desorption than heating at 1°C per minute. In line with this is the more pronounced effect of lowering the heating rate on the Pt dispersion of the Pt/H-USY catalyst than of the Pt/NaY catalyst (Table 4) as the amount of ammonia that needs to be oxidized and/or desorbed is much higher with the ion-exchanged NH_4-USY support than with the NaY support. Furthermore the acid–base interaction of ammonia and protons on the H-USY catalyst slows down the desorption rate compared with that with the NaY catalyst.

An explanation other than autoreduction is needed to explain why a poorly dispersed catalyst is obtained when the sample is heated at 0.2°C per minute but with water added to the gas flow (Pt/NaY(1.1–IE–0.2 water)) (Table 4). Water vapor present in the pores of the zeolite will coordinate to the Pt cations and sites of the cavity walls of the zeolite. It enhances the mobility of the cations in the zeolite. In aqueous solutions the Pt^{2+} ion behaves rather soft acidic with an estimated pK_a value of 2.5 (28). With no ammonia ligands present partial hydrolysis already proceeds at a pH just above unity, and at a pH of 4 a hydroxide-like precipitate is formed (29, 30). Condensation reactions and subsequent precipitation could also well occur in the zeolite, thereby leading to a less dispersed calcined precursor:

$$n\mathrm{Pt(H_2O)_4^{2+}(O_{zeo}^-)_2} \rightarrow \mathrm{Pt}_n\mathrm{O}_{n-x}(\mathrm{OH})_{2x} + (3n-x)\mathrm{H_2O} + (2n)\mathrm{H^+O_{zeo}^-}.$$

It must be noted that in the experiment this condition is forced by excess water. Evidence against a complete precipitation after calcination with dry gases has been obtained from IR studies showing that the majority of the protons are generated after reduction of the precursor (31). However, already a small amount of platinum(hydr)oxide could lead to less dispersed metal as it is able to grow by deposition and catalytic reduction of cationic precursor when treating the sample with hydrogen in the reduction step. The amount of water present at higher temperature in the zeolite due to calcination of precursor or left after the drying treatment at 150°C will be lower when a heating rate of 0.2°C per minute is used instead of 1°C per minute.

One could consider completely avoiding the coordination of ligands to the Pt precursor as was done succesfully on H-ZSM 5 where the presence of bare platinum cations was established (8) after calcination at 450°C. However, the coordination of ligands to Pt^{2+} in zeolite Y is to some extent necessary to keep the precursor in the supercage and to prevent its migration to sodalite sites which results, as mentioned above, in a lower dispersion (4, 27).

Taking into account the necessity of carefully removing ammonia from the ion-exchanged zeolites by calcination to obtain, after reduction, small platinum particles, the use of NH_4-USY to ion-exchange with and prepare Pt/H-USY seems less beneficial than use of H-USY zeolite. However, previous work by our group on the preparation of Pt/Y catalysts by ion exchange with $Pt(NH_3)_4^{2+}$ revealed that the metal dispersion obtained after reduction was progressively lower with increasing Brønsted acidity of the ion-exchanged zeolite.

Preparation of Highly Dispersed Platinum on Zeolite Y by Impregnation

EXAFS analyses revealed highly dispersed platinum on NaY and H-USY prepared by impregnation of respectively NaY and NH_4-USY and calcination at 0.2°C per minute. The average particle size is not much higher than that obtained with the ion-exchanged and reduced zeolites (on average 20 atoms per cluster (IM) versus 13 atoms per cluster (IE)). The size distribution is less homogenous than that obtained with ion exchange as a fraction of the metal is present as larger platinum particles on part of the zeolite crystals. With impregnation of powders the distribution of precursor solution over the support is often a problem. Due to its high sorptive properties the micropores of the zeolite kept in air at RT are completely filled with water (30 wt% water whereas the micropore volume is 0.35 ml per gram). Therefore the zeolite is dried *in situ* first to empty the micropores. Whereas the high capillary forces of the micropores of the zeolite are probably enhancing the sorption of most of the precursor solution inside the zeolite crystals, a part of the precursor liquid is contained in the mesopore volume of NH_4-USY and could as well be contained inbetween powder particle agglomerates of NaY and NH_4-USY. Nonexchanged precursor precipitates on drying as $Pt(NH_3)_4(NO_3)_2$ as the nitrate ions are contained in the sample with impregnation. Furthermore, a (small) part of the precursor is expected to remain dissolved in the precursor solution inside the micropores due to the presence of the cations (Na^+, NH_4^+), and then on drying, migration to the external surface will occur where $Pt(NH_3)_4(NO_3)_2$ precipitates. These processes will lead to large(r) platinum particles. Evidence for the precipitation of precursor and incomplete ion exchange is found in the lower Brønsted acidity of Pt/NaY prepared by impregnation than when prepared by ion exchange, as is concluded from the activities of these catalysts for *n*-heptane isomerization. Whereas ion exchange leads to the generation of two protons per Pt cation after reduction, with calcination and reduction of $Pt(NH_3)_4(NO_3)_2$ no protons are generated.

Preparation on Silica–Alumina versus Zeolite Y

Highly dispersed platinum on amorphous silica–alumina is prepared by impregnation of the support with the Pt precursor solution. The metal dispersion after reduction is not strongly dependent on the heating rate during calcination or on whether the precursor was decomposed or calcined prior to reduction. Whereas the silica–alumina used has a large number of acid sites (Table 1) and the presence of tetrahedrally coordinated aluminum was confirmed by ^{27}Al NMR, the major difference between this support and the zeolites is the absence of micropores. The amount of water sorbed in the material kept in air is only a few percent. The desorption rate of ammonia and water from this porous material is relatively high and therefore no low heating rate is necessary. As a consequence precursor applied on this material is less susceptible to undergo such processes as autoreduction, migration, and possibly precipitation, leading to low dispersed platinum as with the zeolites. In addition, the micropores of the zeolite might well play a role in stabilizing mobile precursor species such as $Pt(NH_3)_2H_2$ (in line with the high H/Pt ratios found for the ion-exchanged zeolites) which is not the case with the silica–alumina.

CONCLUSIONS

In this study the Pt particle size and particle size distribution of Pt/Y and $Pt/SiO_2–Al_2O_3$ catalysts are quantified with a combination of TEM, EXAFS, hydrogen chemisorption, and modeling of Pt particle sizes. A key parameter for the preparation of highly dispersed Pt particles with a narrow particle size distribution in Y zeolite appears to be the heating rate used to calcine the samples. For zeolite Y ion-exchanged with $Pt(NH_3)_4^{2+}$(aq) a rate of 1°C/min as used in the literature already leads to a bimodal particle size distribution. About 5 wt% large particles of 4–9 nm are (partially) occluded in the zeolite; 95 wt% of the Pt particles have an average size of 1–1.2 nm. When the calcination was performed at 0.2°C/min, homogeneously dispersed platinum particles smaller than 1 nm with on average 13 atoms per particle were obtained.

This study shows that it is also possible to prepare highly dispersed Pt particles with a narrow particle size distribution in Y zeolite using the more easily applied impregnation technique. At a heating rate of 0.2°C per minute the average particle size was found to be 1–1.1 nm with only a small fraction of metal present as particles larger than 2 nm.

Highly dispersed platinum particles <1 nm with on average 13 atoms per particle are prepared on mesoporous (amorphous) $SiO_2–Al_2O_3$ by impregnation with $Pt(NH_3)_4^{2+}$(aq). With this support the Pt dispersion is not sensitive to the heating rate used for calcination. This difference is explained by the higher desorption rate of ammonia and water from $SiO_2–Al_2O_3$ which slows down the processes of autoreduction and migration of the precursor.

REFERENCES

1. "Oil and Gas Journal Data Book," Penn Well, Tulsa, OK, 1994.
2. Stakheev, A. Yu., and Kustov, L. M., *Appl. Catal. A* **188**, 3 (1999).
3. Dalla Betta, R. A., and Boudart, M., *in* "Proceedings, 5th International Congress on Catalysis, Palm Beach, 1972" (J. W. Hightower, Ed.), p. 96. North Holland, Amsterdam, 1973.
4. Gallezot, P., *Catal. Rev. Sci. Eng.* **20**, 121 (1979).
5. Homeyer, S. T., and Sachtler, W. M. H., *J. Catal.* **17**, 91 (1989).
6. Jacobs, P. A., *Stud. Surf. Sci. Catal.* **29**, 357 (1986).

7. Reagan, W. J., *J. Catal.* **69**, 89 (1981).
8. Vandenbroek, A. C. M., Van Grondelle, J., and van Santen, R. A., *J. Catal.* **167**, 417 (1997).
9. Kampers, F. W. H., Engelen, C. W. R., van Hooff, J. H. C., and Koningsberger, D. C., *J. Phys. Chem.* **94**, 8574 (1990).
10. Pandya, K. I., Heald, S. M., Hriljac, J. A., Petrakis, L., and Fraissard, J., *J. Phys. Chem.* **100**, 5070 (1996).
11. Bovin, J. O., and Malm, J. O., *Z. Phys. D* **19**, 293 (1991).
12. Ozkaya, D., Zhou, W., Thomas, J. M., Midgley, P., Keast, V. J., and Hermans, S., *Catal. Lett.* **60**, 113 (1999).
13. Petrakis, L., Springuel-Huet, M. A., Ito, T., Hughes, T. R., Chan, I. Y., and Fraissard, J., *in* "Proceedings, 9th International Congress on Catalysis, Calgary, 1988" (M. J. Phillips and M. Ternan, Eds.), p. 348, Chem. Inst. of Canada, Ottawa, 1988.
14. Tonscheidt, A., Ryder, P. L., Jaeger, N. I., and Schulz Ekloff, G., *Zeolites* **16**, 271 (1996).
15. Pan, M., Cowley, J. M., and Chan, I. Y., *Catal. Lett.* **5**, 1 (1990).
16. Kampers, F. W., Maas, T. M. J., van Grondelle, J., Brinkgreve, P., and Koningsberger, D. C., *Rev. Sci. Instrum.* **60**, 2645 (1989).
17. van Zon, J. B. A. D., Koningsberger, D. C., van't Blik, H. F. J., and Sayers, D. E., *J. Chem. Phys.* **12**, 5742 (1985).
18. Koningsberger, D. C., Mojet, B. L., van Dorssen, G. E., and Ramaker, D. E., *Top. Catal.* **10**, 143 (2000).
19. van Dorssen, G. E., Koningsberger, D. C., Ramaker, D. E., submitted for publication.
20. Voogt, E. H., Ramses software, http://www.chem.ruu.nl/opp/www/software/software.html, Debye Institute of Utrecht University, 1996.
21. Koningsberger, D. C., de Graaf, J., Mojet, B. L., Ramaker, D. E., and Miller, J. T., *Appl. Catal. A* **191**, 205 (2000).
22. "Handbook of Chemistry and Physics," 56th ed. CRC Press, Boca Raton, FL, 1975.
23. Boitiaux, J. P., *Rev. Inst. Fr. Petr.* **48**, 527 (1993).
24. Vaarkamp, M., Miller, J. T., Modica, F. S., and Koningsberger, D. C., *J. Catal.* **163**, 294 (1996).
25. Novakova, J., Kubelkova, L., Brabec, L., Bastl, Z., Jaeger, N., and Schulz Ekloff, G., *Zeolites* **16**, 173 (1996).
26. Park, S. H., *Appl. Catal.* **24**, 85 (1986).
27. Homeyer, S. T., and Sachtler, W. M. H., *Zeolites: Facts Figures Future*, 975 (1989).
28. Elding, L. I., *Inorg. Chim. Acta* **20**, 65 (1976).
29. Richens, D. T., "The Chemistry of Aqua Ions." Wiley, New York, 1997.
30. Guerin, M., Kappenstein, C., Alvarez, F., Gianetto, G., and Guisnet, M., *Appl. Catal.* **45**, 325 (1988).
31. Tzou, M. S., Teo, B. K., and Sachtler, W. M. H., *J. Catal.* **113**, 220 (1988).